

Article

NbSe₂ Crystals Growth by Bromine Transport

Dimitre Dimitrov ^{1,2,*}, Peter Rafailov ¹, Vera Marinova ², Ivalina Avramova ³, Daniela Kovacheva ³,
Irnik Dionisiev ², Nikolay Minev ² and Marin Gospodinov ¹

¹ Institute of Solid State Physics, Bulgarian Academy of Sciences, 1784 Sofia, Bulgaria; rafailov@issp.bas.bg (P.R.); maringospodinov@abv.bg (M.G.)

² Institute of Optical Materials and Technologies, Bulgarian Academy of Sciences, 1113 Sofia, Bulgaria; vmarinova@iomt.bas.bg (V.M.); idionisiev@iomt.bas.bg (I.D.); nminev@iomt.bas.bg (N.M.)

³ Institute of General and Inorganic Chemistry, Bulgarian Academy of Sciences, 1113 Sofia, Bulgaria; iva@svr.igic.bas.bg (I.A.)

* Correspondence: dzdimitrov@issp.bas.bg

Abstract: Recently, low-dimensional structures in the form of bulk crystals and nanoflakes have received considerable interest due to their 2D unique functionality and promising applications in electronics, photonics, sensing devices and photovoltaic solar cells. As a result, remarkable efforts and modifications have been made for the synthesis process of crystalline material by the vapor transport technique. Here, an alternative concept of NbSe₂ crystal growth by the chemical vapor transport (CVT) technique using bromine as a vapor transport agent is presented and subsequently analyzed by X-ray diffraction (XRD), Raman and X-ray photoelectron spectroscopy (XPS) spectroscopy. X-ray powder diffraction analysis revealed hexagonal 2H-NbSe₂ and 4H-NbSe₂ phases, and characteristic Raman and XPS spectra typical for crystalline NbSe₂ were obtained. The environmental sensitivity of the grown crystals is manifested by luminescence attributed to oxidized Nb at the samples' surface.

Keywords: transition metal dichalcogenides; NbSe₂ single crystal; Raman spectroscopy; chemical vapor transport



Citation: Dimitrov, D.; Rafailov, P.; Marinova, V.; Avramova, I.; Kovacheva, D.; Dionisiev, I.; Minev, N.; Gospodinov, M. NbSe₂ Crystals Growth by Bromine Transport. *Coatings* **2023**, *13*, 947. <https://doi.org/10.3390/coatings13050947>

Academic Editor: Aivaras Kareiva

Received: 13 April 2023

Revised: 9 May 2023

Accepted: 15 May 2023

Published: 18 May 2023



Copyright: © 2023 by the authors. Licensee MDPI, Basel, Switzerland. This article is an open access article distributed under the terms and conditions of the Creative Commons Attribution (CC BY) license (<https://creativecommons.org/licenses/by/4.0/>).

1. Introduction

Two-dimensional (2D) van der Waals (vdW) materials have unique physical properties and tremendous potential for contemporary applications. The dimensionality effects exhibited by two-dimensional van der Waals materials have recently attracted extensive interest. Due to the weak vdW bonding between the layers, 2D materials can be straightforwardly exfoliated, transferred and stacked using mechanical processes, which provide a perfect platform studying magnetic, electrical, optical, mechanical and various other specific physical properties to the monolayer limit [1,2].

2H-NbSe₂ is particularly actively investigated material among the transition metal dichalcogenides (TMDs). The single crystal 2H-NbSe₂ is reported to be a prototypical anisotropic s-wave superconductor with zero-field critical temperature T_c = 7.2 K, along with an incommensurate charge density wave (CDW) phase at a temperature of T_{CDW} = 33 K. The competitive relationship between the superconducting phase and CDW phase has brought about wide and sustained arguments [3]. In comparison to the bulk counterpart, monolayer NbSe₂ exhibits a strongly enhanced CDW order and intrinsic Ising superconductivity [4]. Due to its specific electric properties, NbSe₂ is anticipated to be a feasible Lego brick for heterojunction device applications, such as high-performance field-effect transistors or superconductor–semiconductor heterostructures for the detection of Majorana fermions [5,6]. 2H-NbSe₂, 4H-NbSe₂ and 3R-NbSe₂ are the three most common polytypes of niobium diselenide. The first two hexagonal structures possess superconductivity below 7.2 K and 6.3 K, respectively. The third rhombohedral structure is not superconducting up to 1.2 K [7]. Therefore, it is very important to establish reliable

techniques for the synthesis of corresponding high-quality crystals and thin layers. Despite there being several bottom-up and top-down methods for obtaining nanolayers, physical and chemical vapor deposition methods are not completely appropriate for synthesizing highly crystalline samples, due to the inevitable substrate- and layer-induced defects (e.g., vacancies, dislocations and grain boundaries) and the attained critical temperatures were currently far below those of the exfoliated sheets [8]. Chemical vapor transport is still the most reliable and low-priced method for growing high-quality TMD single crystals [9,10]. NbSe₂ single crystals are usually grown using the iodine-assisted CVT method [11,12]. Furthermore, it was proposed [13] modified temperature-oscillating CVT method for controllable growth of NbSe₂ single crystals. This kinetic process, functioning by temperature oscillation in a two-zone furnace, was used to maintain a supersaturation-dependent growth. Crystals with screw dislocations as well as homogeneous hexagonal crystals were developed during the oscillation under different cooling rates. It is observed for group VI dichalcogenides that bromine is a more suitable transport additive than iodine. Chemical transport rates with iodine are low; however, transport with bromine is more effective. Moreover, the addition of bromine led to WSe₂ crystals of better quality [14].

In this paper, we report on the growth conditions and characterization of NbSe₂ single crystals by means of bromine vapor transport. The performed X-ray powder diffraction analysis revealed a hexagonal 2H-NbSe₂ phase, afterwards characterized by Raman and XPS analysis.

2. Materials and Methods

The CVT method is a relatively quick and simple growth technique with high yield, which relies on the use of transporting agents such as I₂, Br₂, etc. CVT is a process of crystal growth that generates crystals via gas-phase transport. The target material is combined with a volatile transport agent in a long quartz tube/ampoule sealed under vacuum. When this tube is heated, the transport agent is vaporized. The transport agent then reacts with the target material, transforming it into a gaseous intermediate phase which can then travel along the length of the tube. Once the intermediate reaches the other, typically cooler, end of the tube, the temperature is low enough that there is no longer sufficient thermal energy to maintain the gaseous intermediate. It then decomposes into the transport agent, which remains in the gas phase, and the target material, which deposits on the tube surfaces and crystallizes [15].

NbSe₂ crystals were synthesized from the elemental components in a two-step process by chemical vapor transport. First, for preliminary synthesis of polycrystalline NbSe₂ material, stoichiometric amounts of Nb (purity 99.99%, Alfa Aesar, Haverhill, MA, USA) and Se (purity 99.9%, Alfa Aesar, Haverhill, MA, USA) elemental powders were sealed in a quartz ampoule under vacuum and annealed in a tube furnace at 850 °C for 72 h followed by cooling at 5 °C/min rate down to 350 °C and then removed from the furnace. The reaction product was confirmed by XRD analysis to be polycrystalline NbSe₂. NbSe₂ single crystals were grown by chemical vapor transport CVT technique using bromine vapor transport setup (Figure 1a). For the growth of NbSe₂ crystals, the grounded sintered polycrystalline NbSe₂ and narrow capillary with bromine (~2 mg/cc) of ampoule volume were sealed in an evacuated (10⁻⁵ torr) quartz ampoule for compound preparation. After sealing the loaded ampoule, the NbSe₂ powder and bromine were thoroughly mixed by vigorous shaking. The powder charge along with bromine were kept at one end of the ampoule. The sealed ampoule was introduced horizontally into the two-thermal-zone furnace. The furnace temperature in both the zones increased slowly to 850 °C (hottest, reaction zone) and 800 °C (cooler, growth zone). The ampoule was left at these temperatures for 168 h. After the required period of growth, the furnace was cooled down to room temperature with the rate of 50 °C/h. The ampoule was then broken, and crystals were found to have grown at the cooler end of the ampoule.

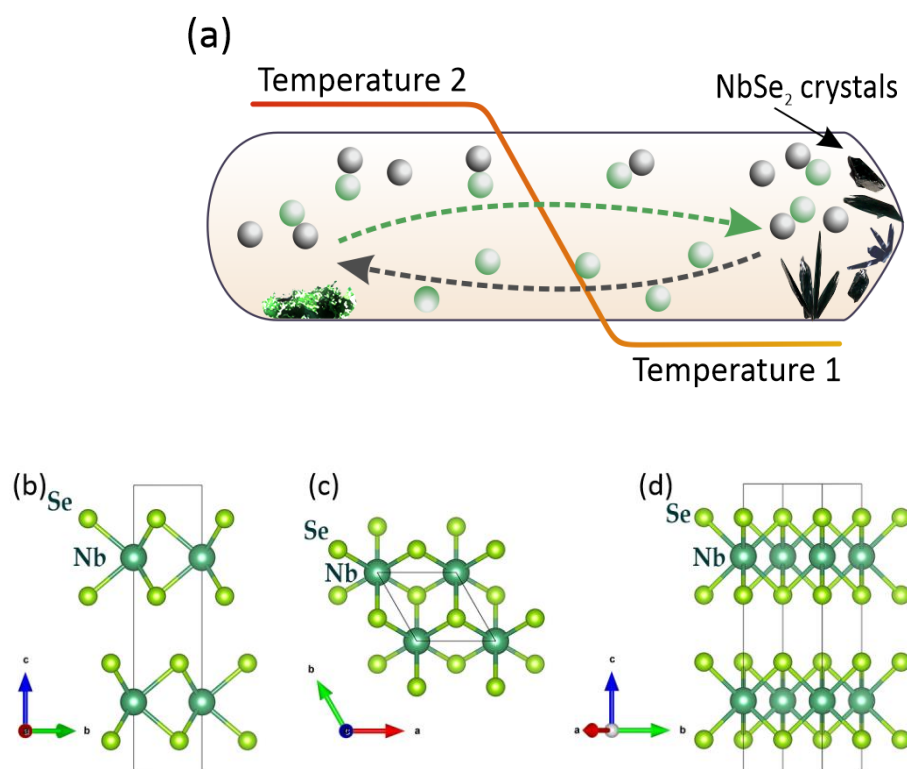


Figure 1. (a) Chemical vapor transport (CVT) method setup used for the growth of NbSe₂ crystal growth and (b–d) schematic crystal structure of 2H-NbSe₂ along the a,b,c axis [16].

In order to completely understand the structure of NbSe₂ samples, a powder X-ray diffraction (PXRD) was performed. Structure analysis by single-crystal X-ray diffraction is one of the most powerful techniques for elucidating solid-state and molecular structures. It provides common detailed information on the lattices of crystalline materials, including unit cell dimensions, bond lengths, bond angles, and details of site ordering. Powder X-ray diffraction patterns were gathered within the 2θ range from 10° to 80° with a constant step 0.02° on a Bruker D8 Advance diffractometer (Billerica, MA, USA) with tube CuK α 40 KV, 40 mA. Goniometer radius 217.5 mm, scan type coupled TwoTheta/Theta, 10° – 80° , step 0.02, counting time 35 s/step, primary Soller slit 4° , divergent slit 0.3° , secondary Soller slit 4° , anti-scattered slit 0.5° , LynxEye detector (Billerica, MA, USA) and detector slit 11.93 mm. Phase identification was performed with the Diffracplus EVA using the ICDD-PDF2 Database (Newtown Square, PA, USA).

The Raman spectra were collected in backscattering geometry at a HORIBA Jobin Yvon Labram HR visible spectrometer (HORIBA France SAS, Lille, France) coupled to a Peltier-cooled CCD detector. A He-Ne laser with wavelength of 632.8 nm was used for excitation with spectral resolution of $\sim 1.5 \text{ cm}^{-1}$. The laser beam was focused on a spot with approximate size of $5 \mu\text{m}$ on the sample surface using a microscope objective with magnification $50\times$. The laser power was attenuated to below $300 \mu\text{W}$ to prevent sample overheating. Raman line parameters were determined from fit to Voigt profiles.

The X-ray photoelectron spectroscopy (XPS) studies were performed in a VG Escalab MKII electron spectrometer (VG Scientific Limited, London, UK) using AlK α radiation with energy of 1486.6 eV under base pressure 10^{-8} Pa and a total instrumental resolution of 1 eV. The binding energies (BE) were determined using the C 1s line as a reference with an energy level of 285.0 eV. The accuracy of the measured BE was 0.2 eV. The photoelectron lines of the constituent elements on the surface were recorded and corrected by subtracting a Shirley-type background and quantified using the peak area and Scofield's photoionization cross-sections. The spectra deconvolution was performed with XPSPEAK41 software (version 4.1).

The excitation source for photoluminescence (PL) spectroscopy setup was a 325 nm line of a He–Cd laser and the emissions were analyzed using a Horiba-Jobin Yvon iHR550 (1800 grooves/mm grating, HORIBA France SAS, Lille, France) spectrometer with a liquid-nitrogen-cooled CCD detector.

3. Results and Discussion

3.1. X-ray Diffraction Analysis (Crystalline Structure)

NbSe₂ has a Molybdenite-like structure and crystallizes in the hexagonal P6₃/mmc space group. The structure is two-dimensional and consists of two NbSe₂ sheets oriented in the (0, 0, 1) direction. In the structure, Nb⁴⁺ is bonded to six equivalent Se²⁻ atoms to form distorted edge-sharing NbSe₆ pentagonal pyramids. All Nb–Se bond lengths are 2.62 Å. Se²⁻ is bonded in a three-coordinate geometry to three equivalent Nb⁴⁺ atoms. Figure 2 shows the X-ray diffraction pattern for powdered NbSe₂ which can be well indexed within the P6₃/mmc structure. According to the X-ray powder diffraction analysis, a hexagonal P6₃/mmc, 2H-NbSe₂ crystalline (JCPDS card no. 01-070-5612) phase (platelets) with lattice cell parameters of $a = 0.345(2)$ nm, $b = 0.345(2)$ nm and $c = 1.253(0)$ nm and a hexagonal P-6m2, 4H-NbSe₂ (JCPDS card no. 01-072-1621) phase with lattice cell parameters of $a = 0.344(9)$ nm, $b = 0.344(9)$ nm and $c = 2.539(3)$ were obtained. In Figure 2, some faint peaks are also detected (marked with asterisks) which match the peaks in the X-ray diffraction pattern of monoclinic [17] NbSe₃ (JCPDS card no. 00-029-0950). This indicates the presence of minor inclusions of crystalline NbSe₃ (needle-like shape) in the studied specimens. It should be mentioned that niobium always contains tantalum in some quantity despite the purity of the product. However, it was found [18] that Ta-doped 2H-NbSe₂ sustains the original structure, yet shows an enhanced electronic property, which could be beneficial to the realization of the superconducting properties of 2H-NbSe₂. Q is for quartz from the quartz ampoule used for CVT growth. Crystals of 2H- and 4H-NbSe₂ were grown at 750 and 925 °C, respectively, from polycrystalline compounds, using the vapor transport technique in [19]. In 2H-NbSe₂, superconducting and charge density wave (CDW) transitions were observed at $T_c = 7.4$ K and $T_{CDW} = 35$ K, respectively. It is found that these two transitions are changed to $T_{CDW} = 42$ K and $T_c = 6.5$ K in 4H-NbSe₂ [19].

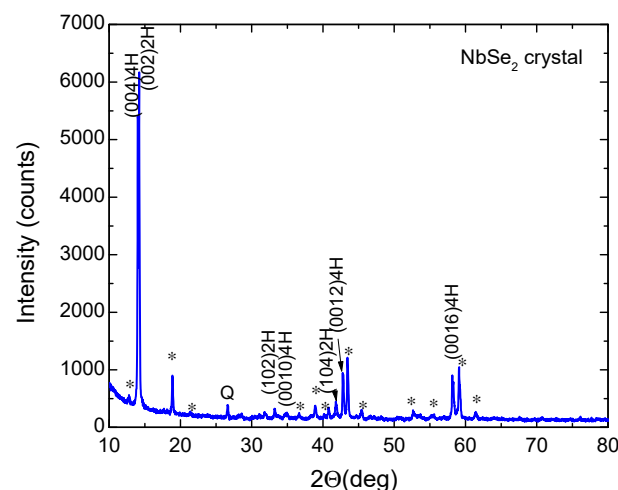


Figure 2. X-ray diffraction patterns of NbSe₂ crystals. NbSe₃ peaks are marked with asterisks.

Figure 3 shows an optical microscopic image of one of the grown crystal specimens that was used for further characterization. From Figure 3, the presence of naturally grown smooth surfaces is evident, whose facets contain angles of 60° and 120° indicating a crystalline hexagonal phase. Due to minor sample tilting, some of these structures are slightly smeared out, therefore several spots where such angles occur are encircled with a white line as a guide to the eye.

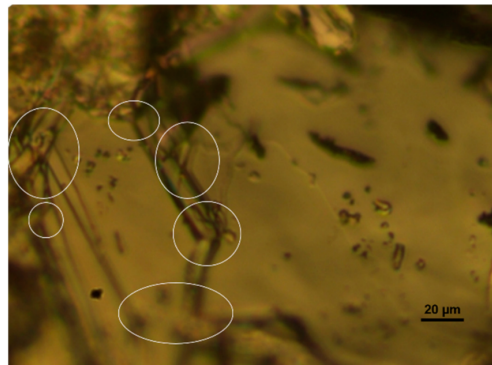


Figure 3. Optical microscopic image of a NbSe₂ crystal surface containing faceted naturally grown surfaces. Some facet edges making angles of 60° and 120° are encircled with a white line for clarity.

3.2. Raman Analysis

Various Raman-active features are expected for the normal phase of 2H-NbSe₂; however, the Raman spectra of materials can be affected by many factors, including the dimensionality effect, impurities and doping. Therefore, we conducted the Raman characterization on a smooth naturally grown surface as shown in Figure 3. For the 2H-NbSe₂ compound [20], the A_{1g} and E_{2g} Raman-active phonons and the so-called soft mode were detected [21–23] as depicted in Figure 4. A_{1g} corresponds to an out-of-plane mode and its spectral line is located at ~230 cm⁻¹. E_{2g} is an in-plane vibration with extremely weak Raman activity upon red excitation [20] and appears at ~239 cm⁻¹ as a faint shoulder at the high-frequency side of the A_{1g} line. The linewidth of the A_{1g} phonon in Figure 4 is only 5 cm⁻¹, indicating the good quality of the obtained NbSe₂ crystal. A quite similar spectrum was published for a NbSe₂ crystal prepared by the flux method in Ref. [24]. For the 2H-NbSe₂ structure, there is also another Raman-active mode—E_{1g}—which is expected at ~134 cm⁻¹ [21]. However, due to the presence of facet edges producing angles of 60° and 120° in Figure 3, it is highly probable that our Raman spectra were taken from the [001] plane of the hexagonal lattice and the E_{1g} line is forbidden in this scattering geometry.

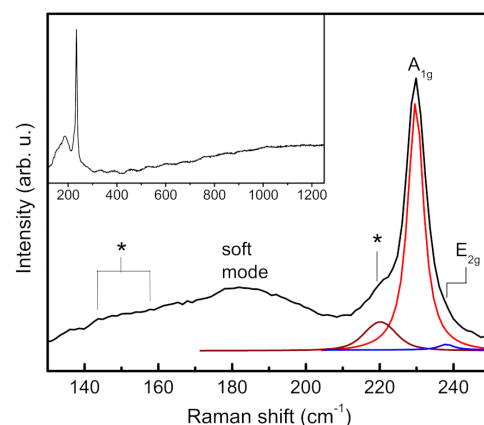


Figure 4. Raman spectra of the studied NbSe₂ crystal. Low-intensity components stemming from NbSe₃ inclusions are marked with asterisks. Fitted peaks are plotted below the spectra for the A_{1g} (red), E_{2g} (blue) and A_g (NbSe₃) (brown) phonons for clarity. Inset: full extension of the NbSe₂ Raman spectrum.

The broad feature centered at ~180 cm⁻¹ (Figure 4) is assigned as “soft mode” and involves a second-order scattering processes of phonons from the periphery of the Brillouin zone, including both intralayer and interlayer vibrations [22,23]. The temperature dependence of this mode has been found to correlate with the CDW transition. It softens significantly upon cooling until reaching T_{CDW}, below which it remains frozen [23].

The spectrum in Figure 4 contains two additional features (marked with asterisks) which are identified as originating from the minor NbSe₃ inclusions in our specimen: a shoulder at the low-frequency side ($\sim 220\text{ cm}^{-1}$) of the A_{1g} line and a feature at about $145\text{--}155\text{ cm}^{-1}$ which may also be viewed as a shoulder to the broad “soft mode” band. The shoulder at 220 cm^{-1} coincides with the strongest A_g Raman line of monoclinic NbSe₃ at $\sim 218\text{ cm}^{-1}$ [17], and the broad feature at $145\text{--}155\text{ cm}^{-1}$ matches the frequency range of the strongest band in the NbSe₃ Raman spectrum consisting of three other A_g lines at 143, 156 and 164 cm^{-1} [17].

In Figure 4, the fit components corresponding to the three first-order phonon lines (A_{1g}, E_{2g} and A_g (NbSe₃)) are plotted below the measured spectrum for clarity. In the inset, the same spectrum is shown in its full extension to above 1200 cm^{-1} .

3.3. X-ray Photoelectron Spectroscopy (XPS)

For the XPS analysis, a small portion of the sample was pressed in a pellet and placed in the analysis chamber. XPS analysis was carried out to investigate the chemical nature and identify the elements present in the NbSe₂ crystal. Figure 5a shows the XPS survey scan. The predominant peaks correspond to Nb 3d, Se 3d, C 1s and O 1s core-level spectra, respectively. As can be seen from the survey scan of NbSe₂ crystals, the Se is predominant on the surface and thus the Auger SeLMM structure is quite extensive and cause spectral interferences with a wide variety of other elements. We did not detect any features typical of Br. The surface concentrations of constituent elements were calculated and are given below as O = 55.47 at.%, Se = 33.04 at.% and Nb = 9.82 at.%, respectively. The spectrum of Nb 3d appeared as a doublet corresponding to Nb 3d_{5/2} and Nb 3d_{3/2} (see Figure 5b). In the present case, this doublet has a complex structure due to the presence of Nb in two different oxidation states, as well overlapping with the SeLMM line. The deconvoluted spectrum of Nb 3d consist of a first doublet with a maximum of around 203.5 eV attributed to the formed Nb-Se bonds and a second doublet with a maximum at 207.5 eV, which corresponds to NbOx. The Se 3d spectrum shows a single peak at 55.1 eV (see Figure 5c).

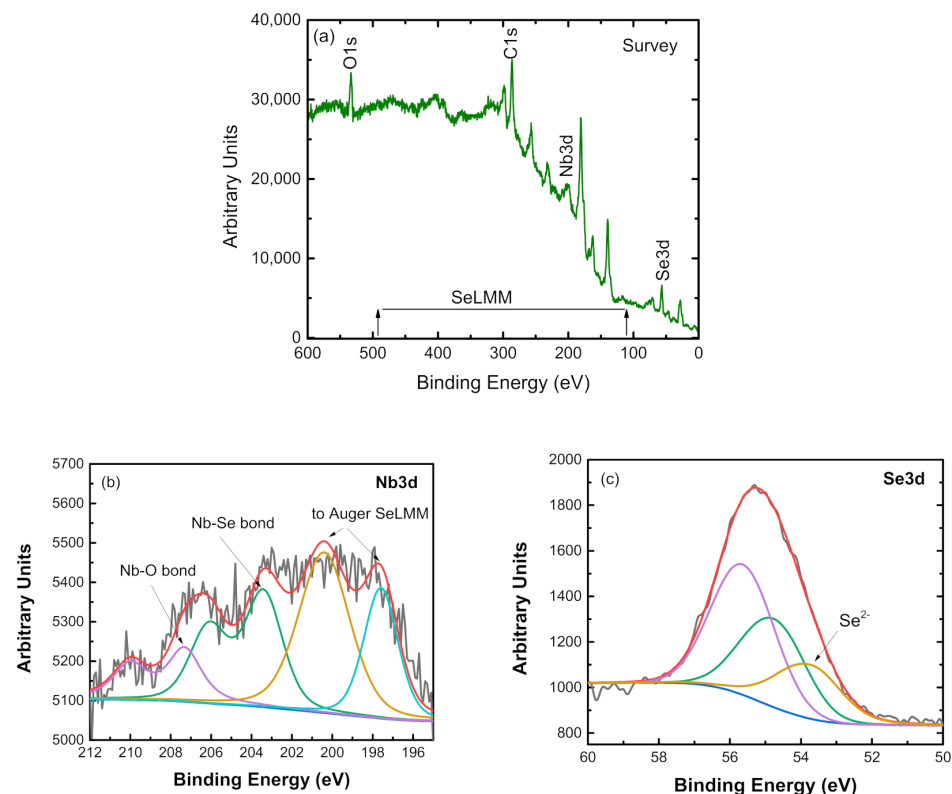


Figure 5. XPS survey scan (a) and spectra of Nb 3d (b) and Se 3d (c).

We should mention here that the Se 3d peak is also a doublet but with a very small spin-orbit splitting (0.86 eV). The Se 3d was fitted with three components. The main components belong to NbSe₂. The other two minor components could be ascribed to residual amorphous Se and/or trigonal Se. The obtained results are compared with data from other literature sources and show the presence of NbSe₂ [25], as well as inevitable surface oxidation [26].

3.4. Photoluminescence

NbSe₂ crystals are recognized for their sensitivity in air [27]. In atmospheric conditions, NbSe₂ already readily oxidizes under very low illumination with very low intensity [28]. Figure 6 shows photoluminescence signals detected at ~2.48 eV (~500 nm) and ~2.95 eV (~420 nm), which are probably related to the (photo)oxidation of Nb to NbO_x (NbO₂, Nb₂O₅), as reported by Ref. [29]. It is observed that the photoluminescence (PL) spectra are visible for the material after 24 h of exposure to air, emphasizing the importance of protection by encapsulation, prompt measurement or the instantaneous placement of crystal samples into an oxygen-free environment as glove-box [30].

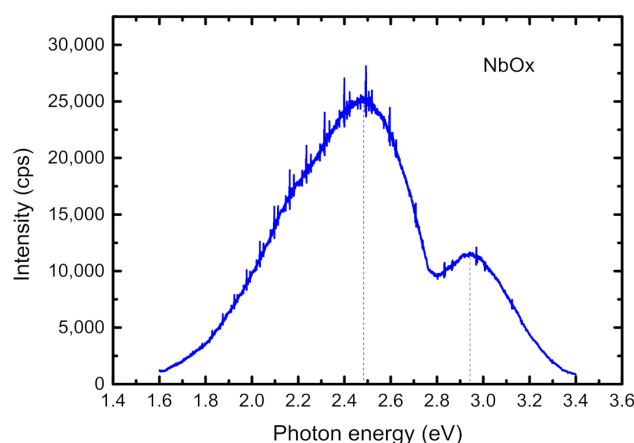


Figure 6. Photoluminescence of (photo) oxidized crystal area.

4. Conclusions

NbSe₂ crystals were grown by the chemical vapor transport (CVT) technique using bromine as the vapor transport agent. The structural and chemical characterization by X-ray powder diffraction, Raman spectroscopy and X-ray photoelectron spectroscopy were performed providing evidence for hexagonal 2H and 4H-NbSe₂ phases and indications of high lattice order and good quality of the obtained crystalline samples. NbSe₂ crystal growth using bromine vapor transport should thus be considered as a reliable option in the development of future technologies for the synthesis of this material.

Author Contributions: Conceptualization D.D. and V.M.; methodology V.M., I.A., D.K., I.D., P.R., M.G. and D.D.; software I.A., I.D., N.M. and P.R.; formal analysis V.M., I.A., P.R., D.K., M.G. and D.D.; resources D.D.; writing—original draft preparation D.D. and V.M.; writing—review and editing V.M., P.R., I.A., D.K. and D.D.; visualization I.D., P.R., I.A. and N.M.; supervision, V.M. and D.D.; funding acquisition D.D. All authors have read and agreed to the published version of the manuscript.

Funding: This research was funded by Bulgarian Science Fund under the projects KII-06-KOCT/13 “Synthesis and characterization of ferromagnetic 3D and 2D Van der Waals materials” and KII-06-H-28/8, and under the COST Action CA 17123 “Ultrafast opto-magneto-electronics for non-dissipative information technology”.

Institutional Review Board Statement: Not applicable.

Informed Consent Statement: Not applicable.

Data Availability Statement: The data presented in this study are available on reasonable request from the corresponding author.

Acknowledgments: Bulgarian Science Fund project KII-06-KOCT/13 “Synthesis and characterization of ferromagnetic 3D and 2D Van der Waals materials” and COST Action CA 17123 “Ultrafast opto-magneto electronics for non-dissipative information technology”. P.R., V.M. and N.M. acknowledge the financial support by the European Regional Development Fund within the Operational Programme ‘Science and Education for Smart Growth 2014–2020’ under the Project CoE ‘National Center of Mechatronics and Clean Technologies’ BG05M2OP001-1.001-0008-C01.

Conflicts of Interest: The authors declare no conflict of interest.

References

1. Das, S.; Robinson, J.A.; Dubey, M.; Terrones, H.; Terrones, M. Beyond Graphene: Progress in Novel Two-Dimensional Materials and van der Waals Solids. *Annu. Rev. Mater. Res.* **2015**, *45*, 1–27. [CrossRef]
2. Bian, R.; Li, C.; Liu, Q.; Cao, G.; Fu, Q.; Meng, P.; Zhou, J.; Liu, F.; Liu, Z. Recent progress in the synthesis of novel two-dimensional van der Waals materials. *Natl. Sci. Rev.* **2022**, *9*, nwab164. [CrossRef] [PubMed]
3. Hossain, M.; Zhao, Z.; Wen, W.; Wang, X.; Wu, J.; Xie, L. Recent Advances in Two-Dimensional Materials with Charge Density Waves: Synthesis, Characterization and Applications. *Crystals* **2017**, *7*, 298. [CrossRef]
4. Tsen, A.W.; Hunt, B.; Kim, Y.D.; Yuan, Z.J.; Jia, S.; Cava, R.J.; Hone, J.; Kim, P.; Dean, C.R.; Pasupathy, A.N. Nature of the quantum metal in a two-dimensional crystalline superconductor. *Nat. Phys.* **2015**, *12*, 208. [CrossRef]
5. He, W.-Y.; Zhou, B.T.; He, J.J.; Yuan, N.F.Q.; Zhang, T.; Law, K.T. Magnetic field driven nodal topological superconductivity in monolayer transition metal dichalcogenides. *Commun. Phys.* **2018**, *1*, 40. [CrossRef]
6. Kim, A.R.; Kim, Y.; Nam, J.; Chung, H.-S.; Kim, D.J.; Kwon, J.-D.; Park, S.W.; Park, J.; Choi, S.Y.; Lee, B.H.; et al. Alloyed 2D Metal–Semiconductor Atomic Layer Junctions. *Nano Lett.* **2016**, *16*, 1890–1895. [CrossRef]
7. Andreeva, O.; Braude, I.; Mamalui, A. Selenium vacancies and their effect on the fine structure of NbSe₂ quasi-two-dimensional single crystals. *Phys. Met. Metallogr.* **2012**, *113*, 888–892. [CrossRef]
8. Dasadia, A.; Bhavsar, V. Growth, structure, electrical and optical properties of transition metal chalcogenide crystals synthesized by improved chemical vapor transport technique for semiconductor technologies. *Prog. Cryst. Growth Charact. Mater.* **2022**, *68*, 100578. [CrossRef]
9. Brixner, L.H. Preparation and properties of the single crystalline AB₂-type selenides and tellurides of niobium, tantalum, molybdenum and tungsten. *J. Inorg. Nucl. Chem.* **1962**, *24*, 257–263. [CrossRef]
10. Kershaw, R.; Vlasse, M.; Wold, A. The preparation of and electrical properties of niobium selenide and tungsten selenide. *Inorg. Chem.* **1967**, *6*, 1599–1602. [CrossRef]
11. Oglesby, C.S.; Bucher, E.; Kioc, C.; Hohi, H. Growth of faceted niobium diselenide. *J. Cryst. Growth* **1994**, *137*, 289–294. [CrossRef]
12. Klemm, R.A. Pristine and intercalated transition metal dichalcogenide superconductors. *Phys. C Supercond. Its Appl.* **2015**, *514*, 86–94. [CrossRef]
13. Li, Z.; Xi, X.; Ding, B.; Li, H.; Liu, E.; Yao, Y.; Wang, W. Thermodynamics and kinetics synergy for controlled synthesis of 2D van der Waals single-crystal NbSe₂ via modified Chemical Vapor Transport. *Cryst. Growth Des.* **2020**, *20*, 706–712. [CrossRef]
14. Schmidt, M.; Gooth, J.; Binnewies, M. Preparation and crystal growth of transition metal dichalcogenides. *Z. Anorg. Allg. Chem.* **2020**, *646*, 1183–1194. [CrossRef]
15. Binnewies, M.; Glaum, R.; Schmidt, M.; Schmidt, P. *Chemical Vapor Transport Reactions*; De Gruyter: Berlin, Germany, 2012.
16. Momma, K.; Izumi, F. VESTA 3 for three-dimensional visualization of crystal, volumetric and morphology data. *J. Appl. Crystallogr.* **2011**, *44*, 1272–1276. [CrossRef]
17. Chen, H.; Ma, Z.; Shao, Y.; Rehman, Z.; Zhang, K.; He, Q.; Song, L. Angle-/temperature-dependence of Raman scattering in layered NbSe₃ crystal. *AIP Adv.* **2017**, *7*, 095316. [CrossRef]
18. Li, H.; Liu, S.; Chen, L.; Wu, J.; Zhang, P.; Tang, H.; Li, C.; Liu, X.; Wang, Z.; Meng, J. Atomic structures and electronic properties of Ta-doped 2H-NbSe₂. *RSC Adv.* **2014**, *4*, 57541–57546. [CrossRef]
19. Naik, I.; Rastogi, A.K. Charge density wave and superconductivity in 2H- and 4H-NbSe₂: A revisit. *Pramana-J. Phys.* **2011**, *76*, 957–963. [CrossRef]
20. Hill, H.M.; Rigosi, A.F.; Krylyuk, S.; Tian, J.; Nguyen, N.V.; Davydov, A.V.; Newell, D.V.; Hight Walker, A.R. Comprehensive optical characterization of atomically thin NbSe₂. *Phys. Rev. B* **2018**, *98*, 165109. [CrossRef]
21. Zhang, X.; Tan, Q.-H.; Wu, J.-B.; Shi, W.; Tan, P.-H. Review on the Raman spectroscopy of different types of layered materials. *Nanoscale* **2016**, *8*, 6435–6450. [CrossRef]
22. Staley, N.E.; Wu, J.; Eklund, P.; Liu, Y.; Li, L.; Xu, Z. Electric field effect on superconductivity in atomically thin flakes of NbSe₂. *Phys. Rev. B* **2009**, *80*, 184505. [CrossRef]
23. Xi, X.; Zhao, L.; Wang, Z.; Berger, H.; Forró, L.; Shan, J.; Mak, K.F. Strongly enhanced charge-density-wave order in monolayer NbSe₂. *Nat. Nanotechnol.* **2015**, *10*, 765–769. [CrossRef] [PubMed]
24. 2Dsemiconductors USA. Available online: <https://www.2dsemiconductors.com/niobium-diselenide-nbse2/> (accessed on 12 April 2023).

25. Calavale, F.; Dreher, P.; Surdendran, A.P.; Wan, W.; Timpel, M.; Verucchi, R.; Rogero, C.; Bauch, T.; Lombardi, F.; Casanova, F.; et al. Tailoring Superconductivity in Large-Area Single-Layer NbSe₂ via Self-Assembled Molecular Adlayers. *Nano Lett.* **2021**, *21*, 136–143. [[CrossRef](#)] [[PubMed](#)]
26. Ahmad, H.M.N.; Ghosh, S.; Dutta, G.; Maddaus, A.G.; Tsavalas, J.G.; Hollen, S.; Song, E. Effects of impurities on the electrochemical characterization of liquid-phase exfoliated niobium diselenide nanosheets. *J. Phys. Chem. C* **2019**, *123*, 8671–8680. [[CrossRef](#)]
27. El-Bana, M.S.; Wolverson, D.; Russo, S.; Balakrishnan, G.; Paul, D.M.; Bending, S.J. Superconductivity in two dimensional NbSe₂ field effect transistors. *Supercond. Sci. Technol.* **2013**, *26*, 125020. [[CrossRef](#)]
28. Holler, J.; Bauried, L.; Korn, T.; Seitz, A.; Özyigit, F.; Eichinger, M.; Schüller, C.; Watanabe, K.; Taniguchi, T.; Strunk, C.; et al. Air tightness of hBN encapsulation and its impact on Raman spectroscopy of van der Waals materials. *2D Mater.* **2020**, *7*, 015012. [[CrossRef](#)]
29. Huang, B.X.; Wang, K.; Church, J.S.; Li, Y.-S. Characterization of oxides on niobium by Raman and infrared spectroscopy. *Electrochim. Acta* **1999**, *44*, 2571–2577. [[CrossRef](#)]
30. Rigosi, A.F.; Hill, H.M.; Krylyuk, S.; Nguyen, N.V.; Hight Walker, A.R.; Davydov, A.V.; Newell, D.B. Dielectric Properties of Nb_xW_{1-x}Se₂ Alloys. *J. Res. Natl. Inst. Stand. Technol.* **2019**, *124*, 124035. [[CrossRef](#)]

Disclaimer/Publisher’s Note: The statements, opinions and data contained in all publications are solely those of the individual author(s) and contributor(s) and not of MDPI and/or the editor(s). MDPI and/or the editor(s) disclaim responsibility for any injury to people or property resulting from any ideas, methods, instructions or products referred to in the content.